AD-A039 087 FRANK J SEILER RESEARCH LAB UNITED STATES AIR FORCE --ETC F/G 10/3
EXPERIMENTAL OPTIMIZATION AND CHARACTERIZATION OF A LIAL/NAALCL--ETC(U)
FEB 77 J C NARDI, J K ERBACHER, C L HUSSEY

UNCLASSIFIED FJSRL-TR-77-0002 NL

1 OF 1
ADA039087

END

DATE FILMED
5 - 77

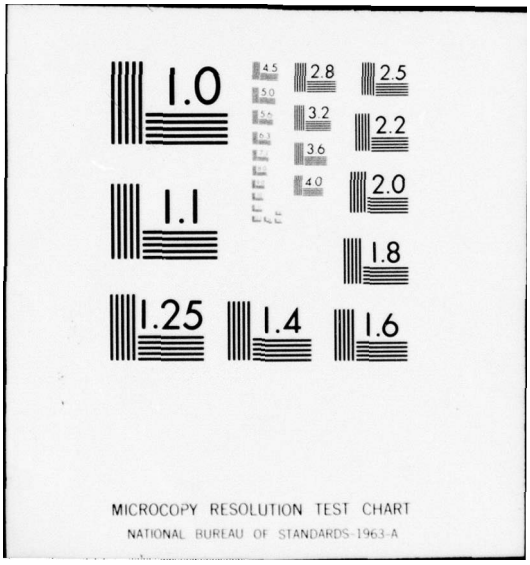
1.0
1.1
1.25
1.4
1.6
1.8
2.0
2.2
2.5
2.8
3.2
3.6
4.0
4.5
5.0
MICROCOPY RESOLUTION TEST CHART
NATIONAL BUREAU OF STANDARDS-1963-A

(12)
BS.

FRANK J. SEILER RESEARCH LABORATORY

FJSRL TECHNICAL REPORT -77-0002
FEBRUARY 1977

EXPERIMENTAL OPTIMIZATION AND CHARACTERIZATION OF A $LiAl/NaAlCl_4/MoCl_5$ PELLETIZED THERMAL CELL

PROJECT 2303

AIR FORCE SYSTEMS COMMAND
UNITED STATES AIR FORCE

NOTICE

When government drawings, specifications, or other data are used for any purpose other than in connection with a definitely related government procurement operation, the United States Government thereby incurs no responsibility nor any obligation whatsoever; and the fact that the government may have formulated, furnished, or in any way supplied the said drawings, specifications, or other data, is not to be regarded by implication or otherwise as in any manner licensing the holder or any other person or corporation, or conveying any rights or permission to manufacture, use, or sell any patented invention that may in any way be related thereto.

Inquiries concerning this document should be addressed to the Frank J. Seiler Research Laboratory (FJSRL/NC), U. S. Air Force Academy, Colorado 80840. Phone - 303/472-2655.

Copies of this report should not be returned unless return is required by security considerations, contractual obligations, or notice on a specific document.

Printed in the United States of America
Available from
National Technical Information Service
U.S. Department of Commerce
5285 Port Royal Road
Springfield, Virginia 22151

UNCLASSIFIED

SECURITY CLASSIFICATION OF THIS PAGE (When Data Entered)

REPORT DOCUMENTATION PAGE	READ INSTRUCTIONS BEFORE COMPLETING FORM
1. REPORT NUMBER: FJSRL-TR-77-0002	2. GOVT ACCESSION NO.: ADA
	3. RECIPIENT'S CATALOG NUMBER
4. TITLE (and Subtitle): Experimental Optimization and Characterization of a LiAl/$NaAlCl_4$/$MoCl_5$ Pelletized Thermal Cell,	5. TYPE OF REPORT & PERIOD COVERED: Technical Report, June 1975-February 1977,
	6. PERFORMING ORG. REPORT NUMBER
7. AUTHOR(s): John C. Nardi, John K. Erbacher, Charles L. Hussey, Lowell A. King	8. CONTRACT OR GRANT NUMBER(s)
9. PERFORMING ORGANIZATION NAME AND ADDRESS: F.J. Seiler Research Laboratory (FJSRL/NC), Air Force Systems Command, US Air Force Academy, Colorado 80840	10. PROGRAM ELEMENT, PROJECT, TASK AREA & WORK UNIT NUMBERS: 61102F/2303/F2/07
11. CONTROLLING OFFICE NAME AND ADDRESS: F.J. Seiler Research Laboratory (FJSRL/NC), Air Force Systems Command, US Air Force Academy, Colorado 80840	12. REPORT DATE: February 1977
	13. NUMBER OF PAGES: 35 (44 P.)
14. MONITORING AGENCY NAME & ADDRESS (if different from Controlling Office): 16 2303, 17 F2	15. SECURITY CLASS. (of this report): Unclassified
	15a. DECLASSIFICATION/DOWNGRADING SCHEDULE: N/A

16. DISTRIBUTION STATEMENT (of this Report)

Approved for public release; distribution unlimited.

17. DISTRIBUTION STATEMENT (of the abstract entered in Block 20, if different from Report)

18. SUPPLEMENTARY NOTES

19. KEY WORDS (Continue on reverse side if necessary and identify by block number)

Thermal Battery
Aluminum Chloride
Molybdenum Pentachloride
Lithium Aluminum Alloys
Tetrachloroaluminate
Reserve Battery
Aluminum

319920 B

20. ABSTRACT (Continue on reverse side if necessary and identify by block number)

A new molten salt thermally activated reserve battery utilizing immobilized liquid $NaAlCl_4$ as the electrolyte is described. Lithium-aluminum alloys are employed as anodes with a cathode of $MoCl_5$ in intimate contact with a powdered graphite current collector. The optimization of the battery with respect to anode, electrolyte and catholyte composition was investigated. Battery discharge behavior was characterized, defining optimum conditions of temperature and discharge rate to produce maximum energy output. The optimal cell configuration delivered 38 W-hr/lb at a discharge rate of 15 mA/cm² at 175°C. The

DD FORM 1 JAN 73 1473 EDITION OF 1 NOV 65 IS OBSOLETE

UNCLASSIFIED SQUARE CM

SECURITY CLASSIFICATION OF THIS PAGE (When Data Entered)

first application of a derivative discharge function to thermal cell analysis characterizes the complex discharge mechanism.

EXPERIMENTAL OPTIMIZATION AND CHARACTERIZATION OF A $LiAl/NaAlCl_4/MoCl_5$ PELLETIZED THERMAL CELL

John C. Nardi
John K. Erbacher
Charles L. Hussey
Lowell A. King

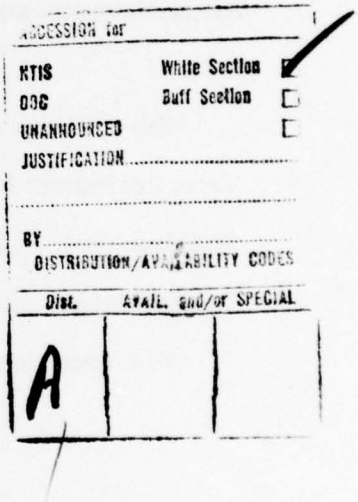

TECHNICAL REPORT SRL-TR-77-0002

February 1977

Director of Chemical Sciences
Frank J. Seiler Research Laboratory
Air Force Systems Command
US Air Force Academy, Colorado 80840

FOREWORD

This report was prepared by the Directorate of Chemical Sciences, Frank J. Seiler Research Laboratory, United States Air Force Academy, Colorado. The work was initiated under Project No. 2303, "Chemistry," Task 2303-F2, "Physical Chemistry and Electrochemistry," Work Unit No. 2303-F2-07, "Pelletized Thermal Batteries."

The report covers work conducted from June 1975 to February 1977. The manuscript was released by the authors for publication in February 1977.

The authors acknowledge the helpful discussions they received from Professor R. A. Osteryoung of Colorado State University, Fort Collins, Colorado; and from D. M. Bush and B. H. Van Domelen at Sandia Laboratories, Albuquerque, New Mexico.

This technical report has been reviewed and approved.

BEN A. LOVING, LtCol, USAF
Director, Directorate of Chemical Sciences

TABLE OF CONTENTS

FIGURES

TABLES

INTRODUCTION

A thermal battery is a primary battery whose cells contain an electrolyte that is solid and non-conductive at ambient temperatures but when melted becomes ionically conductive. A pyrotechnic heat source, once ignited, thermally activates the battery by melting the solid electrolyte. These characteristics make thermal batteries capable of essentially unlimited storage life, rapid and reliable activation, and the ability to withstand high spin rates, severe shock, and vibrations. Therefore, they are able to fulfill certain military, aerospace, and emergency applications.

Thermal batteries are based on a fused salt electrolyte system. Investigations by various workers (1-6) indicate relatively few electrochemical systems for thermal battery use which are capable of achieving high energy density. Thermal batteries presently in production use a LiCl-KCl or LiBr-KBr electrolyte. They operate at high temperatures (400-600^{o}C), thereby incurring at least one inherent disadvantage (7). The disadvantages of high temperature operation have led us to investigate a low temperature electrochemical system for use in high energy density thermal batteries.

Of the electrochemical systems having potential use in thermal batteries (7), aluminum chloride-alkali chloride mixtures (8) are one of the few classes of inorganic molten salts that form relatively low melting compositions. Because they are also good ionic conductors (9), their use as battery electrolytes would lessen problems associated with high operating temperatures of present molten salt electrolyte systems, while retaining the advantage of high energy density. A specific $AlCl_3$

electrolyte that has received considerable attention in our laboratory is the NaCl-saturated $AlCl_3$-NaCl, which has a calculated specific conductivity of 0.4074 mho-cm^{-1} at 175°C (10) and a measured melting point of 158°C.

Prior single cell studies (11) in our laboratory of various anode-cathode couples in $AlCl_3$-NaCl electrolytes showed the LiAl/$MoCl_5$ couple to be a viable high energy density, high discharge rate cell. Studies have been conducted on the preparation of molybdenum (12-13) and the electrochemistry of several molybdenum salts (14-15) in various electrolytes. There have been a few references to the use of molybdenum compounds in battery systems (16-20), but no reported application of molybdenum pentachloride to a thermal battery system.

It was evident from the results of single cell discharge data that varying the anode, electrolyte, and catholyte compositions had a significant effect on overall output and cell efficiency. From the continuous recording of the cell voltage during constant current discharge of the single cells we noted that the LiAl/$NaAlCl_4$/$MoCl_5$ electrochemical system has a complex discharge reaction mechanism. We used a method proposed by Balewski and Brenet (21) to examine the cell discharge mechanism. The use of the derivative of the discharge curve is the first application of this method to thermal battery analysis.

EXPERIMENTAL

Electrolyte preparation, pellet fabrication and cell discharge experiments were described previously (11,22). All experiments were carried out in a Vacuum/Atmospheres Company HE-43-6 Dri-Lab equipped with a HE-493 Dri Train.

Anode: Lithium-aluminum alloys--48.0 a/o powder, 60.2 a/o powder, and 90.9 a/o sheet--were obtained from the Foote Mineral Company and used without further treatment. Preliminary samples of the 48.0 a/o and 90.9 a/o LiAl alloys were secured courtesy of Mr. R. Hudson (Eagle-Picher Industries, Inc.) and Dr. G. Overall (Foote Mineral Co.) respectively. 99.9% pure powdered aluminum was purchased from Research Organics/ Inorganics Chemical Corp.

Catholyte: 99.5% pure anhydrous $MoCl_5$ (Research Organics/Inorganics Chemical Corp., Catalog No. MO-13), was purchased in granular form and separated by particle size with >30, 30-50, 50-100, and <100 ASTM mesh sieves. Graphite (Grade #38) was used as obtained from the Fisher Scientific Co. Superior graphite flakes were purified at 600°C under a chlorine atmosphere using a procedure developed in this laboratory (8).

Current Collectors: Five mil nickel foil (Alfa-Ventron, Inc.), 99.98% pure, was cut into 1.125 inch diameter circles with tab. The collectors were burnished with emery paper, washed with water and acetone, and again lightly burnished before use.

Pellet-Fabrication: Three-layer pellets were formed in all cases when using powdered anode material (Figure 1). Two-layer pellets were used with 90.9 a/o sheet LiAl alloy anodes. The assembled pellets were clamped between the platens at 4.5 lb/in^2.

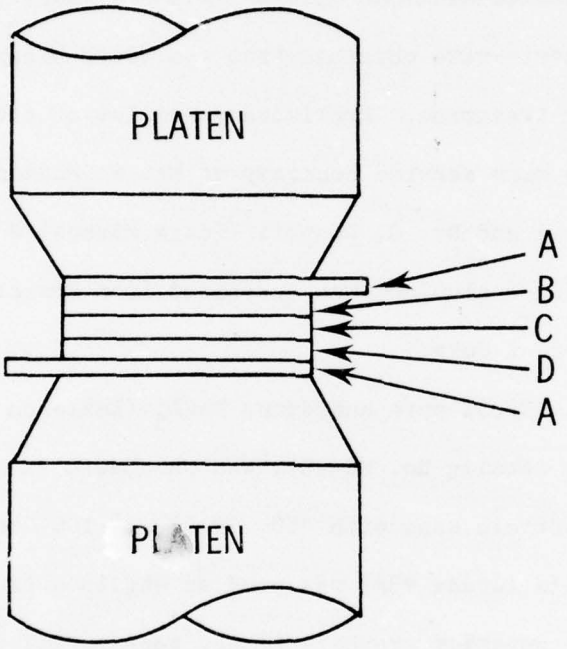

A - current collectors

B - anode

C - electrolyte

D - catholyte

Figure 1. Typical Cell Configuration Between Heated Platens

RESULTS AND DISCUSSION

Single Cell Tests: Single cell tests can be used as a semi-quantitative indicator of the behavior to be expected in a multicell (battery) configuration. An error analysis (23) was performed using the optimized cell configuration (Table I) according to the following equation:

$$\text{relative error} = \sqrt{\frac{(0.01W)^2}{(W)^2} + \sum \frac{(0.005)^2}{(W_i)^2}}$$

where W is the total weight of the pellet and W_i are the individual weights of the single cell components. If one assumes an allowable 1% error in total weight of the pellet and 0.005 gram deviation for the weight of any individual component, the single cell test data have a relative error of 3.25%. The uncertainty in platen press pressure was 4.5 psia $\pm$ 5%. Whether these two errors are additive is unknown. In the LiCl-KCl system, Bush (24) states that at pressures above 1.75 psia cell performance is independent of platen press pressures.

The calculated energy density (watt-hours per pound) in Tables II-VIII were determined from the constant current discharge data using an equation previously described (11).

Cell Configuration: The first experiments were concerned with optimizing the weight ratios for the single cell components to give the maximum energy density output. The weight of only one variable was changed in an experiment in order to realize the effect on overall cell performance. Variables considered were the weight of the anode, weight of separating electrolyte, and the individual weights of electrolyte, $MoCl_5$, and graphite in the catholyte. A typical set of experimental results for a

TABLE I. OPTIMIZED CELL COMPONENT CONFIGURATION

Anode:	0.27 g LiAl (60.2 a/o)
Separator:	0.78 g 90 w/o electrolyte[a]-10 w/o Cab-O-sil
Catholyte:	0.64 g 90 w/o electrolyte[a]-10 w/o Cab-O-sil
	0.72 g $MoCl_5$ (30-50 mesh size)
	0.23 g graphite (Fisher)

[a]Electrolyte consists of 49.85 m/o $AlCl_3$-50.15 m/o NaCl

TABLE II. OPTIMIZATION OF GRAPHITE WEIGHT: 15 mA/cm^2, 200^oC[a]

Graphite Weight (g)	Charge (coul)	Energy Density (W-Hr/lb)
.18	500.4	29.1
.21	523.5	28.2
.23	581.2	31.4
.25	563.9	29.4
.27	548.5	28.4

[a]Cell Configuration:

Anode	.27 g LiAl (60.2 a/o)
Separator	.78 g 90 w/o electrolyte[b]-10 w/o Cab-O-Sil
Catholyte	.64 g 90 w/o electrolyte[b]-10 w/o Cab-O-Sil
	.72 g $MoCl_5$ (30-50 mesh)

[b]Electrolyte consists of 49.85 m/o $AlCl_3$-50.15 m/o NaCl

TABLE III. OPTIMIZATION OF LiAl COMPOSITION: 25 mA/cm^2, 200°C[a]

LiAl a/o	Charge (coul)	Energy Density (W-Hr/lb)
48.0	568	34.6
60.2	609	37.0
90.9	619	33.5

[a]Cell Configuration:

Anode	.27 g LiAl
Separator	.78 g 90 w/o electrolyte[b]-10 w/o Cab-O-Sil
Catholyte	.64 g 90 w/o electrolyte[b]-10 w/o Cab-O-Sil
	.72 $MoCl_5$ (30-50 mesh)
	.23 graphite

[b]Electrolyte consists of 49.85 m/o $AlCl_3$-50.15 m/o NaCl

TABLE IV. OPTIMIZATION OF $MoCl_5$ PARTICLE SIZE: 15 mA/cm^2, 200°C[a]

Particle Size	Charge (coul)	Energy Density (W-Hr/lb)
>30	483.1	24.2
30-50	458.0	22.2
50-100	413.0	17.4
<100	365.8	16.9

[a]Cell Configuration:

Anode	.34 g LiAl (60.2 a/o)
Separator	.82 g 90 w/o electrolyte[b]-10 w/o Cab-O-Sil
Catholyte	.64 g 90 w/o electrolyte[b]-10 w/o Cab-O-Sil
	.72 g $MoCl_5$
	.23 g graphite

[b]Electrolyte consists of 49.85 m/o $AlCl_3$-50.15 m/o NaCl

TABLE V. OPTIMIZATION OF ANODE WEIGHT: 15 mA/cm^2, 200°C[a]

Anode Weight (g)	Charge (coul)	Energy Density (W-Hr/lb)
.27	513.9	27.6
.29	475.3	26.3
.34	458.1	22.2
.43	496.5	19.8

[a]Cell Configuration:

Anode	LiAl (60.2 a/o)
Separator	.82 g 90 w/o electrolyte[b]-10 w/o Cab-O-Sil
Catholyte	.64 g 90 w/o electrolyte[b]-10 w/o Cab-O-Sil
	.72 g $MoCl_5$ (30-50 mesh)
	.23 g graphite

[b]Electrolyte consists of 49.85 m/o $AlCl_3$-50.15 m/o NaCl

TABLE VI. OPTIMIZATION OF SEPARATING ELECTROLYTE WEIGHT: 15 mA/cm^2,200°C[a]

Electrolyte Weight (g)	Charge (coul)	Energy Density (W-Hr/lb)
.74	567.8	30.6
.78	581.2	31.4
.82	475.3	27.6
.99	307.9	11.9

[a]Cell Configuration:

Anode .27 g LiAl (60.2 a/o)

Catholyte .64 g 90 w/o electrolyte[b]-10 c/o Cab-O-Sil

.72 g $MoCl_5$ (30-50 mesh)

.23 g graphite

[b]Electrolyte consists of 49.85 m/o $AlCl_3$-50.15 m/o NaCl

TABLE VII. OPTIMIZATION OF ELECTROLYTE WEIGHT IN CATHOLYTE: 15 mA/cm^2, 200°C[a]

$NaAlCl_4$ Weight (g)	Charge (coul)	Energy Density (W-Hr/lb)
.51	454.2	27.2
.58	381.1	21.1
.64	581.2	31.4
.77	421.5	24.1
.90	392.6	22.4

[a]Cell Configuration:

Anode	.27 g LiAl (60.2 a/o)
Separator	.78 g 90 w/o electrolyte[b]-10 w/o Cab-O-Sil
Catholyte	.72 g $MoCl_5$ (30-50 mesh)
	.23 g graphite

[b]Electrolyte consists of 49.85 m/o $AlCl_3$-50.15 m/o NaCl

TABLE VIII. OPTIMIZATION OF $MoCl_5$ WEIGHT: 15 mA/cm^2, 200°C[a]

$MoCl_5$ (30-50 mesh) Weight (g)	Charge (coul)	Energy Density (W-Hr/lb)
.52	525.4	28.7
.72	581.2	31.4
.79	569.7	31.3
.86	515.8	27.8
.94	563.9	32.6
1.00	525.4	30.4

[a]Cell Configuration:

Anode	.27 g LiAl (60.2 a/o)
Separator	.78 g 90 w/o electrolyte[b]-10 w/o Cab-O-Sil
Catholyte	.64 g 90 w/o electrolyte[b]-10 w/o Cab-O-Sil
	.23 g graphite

[b]Electrolyte consists of 49.85 m/o $AlCl_3$-50.15 m/o NaCl

one component optimization is shown in Table II. A graphite weight of 0.23 grams was selected since it gave the highest coulombic and energy density output during cell discharge to zero volts. A similar set of experiments was conducted for each cell component (Tables III-VIII).

During the optimization of the anode weight, we observed an increase in energy density output as the weight of the LiAl anode was decreased (Table V). Anodes weighing less than 0.27 g could not be fabricated using the available Carver die. Subsequent calculations will show that, assuming the aluminum anode, the anode weight could be reduced even further, with an increase in cell performance.

Anodes prepared from pure aluminum and from 48.0 a/o, 60.2 a/o, and 90.9 a/o LiAl alloys were coupled with the $MoCl_5$ cathode. Cell output was greatly enhanced by using LiAl alloys rather than pure aluminum (Figure 2). This phenomena has also been observed in our electrolyte with various other cathodes (11). This may result from (a) the lithium preventing formation of an insulating oxide layer on the aluminum electrode, (b) the lithium reacting with the oxide layer, or (c) the coupling of the cathode with elemental lithium contained in the alloy material. A comparison of the voltage-time curves during heating of the platens prior to discharge shows an initial high voltage spike (Figure 3A) that is probably due to the $Li/MoCl_5$ couple. This voltage spike is absent when using a pure aluminum anode (Figure 3B).

It was observed that the spike reached a maximum between 150-160°C, the melting range of the electrolyte. The presence of a sharp spike correlated positively with good quality single cell output characteristics. Voltage spiking before discharge has been observed in this laboratory with

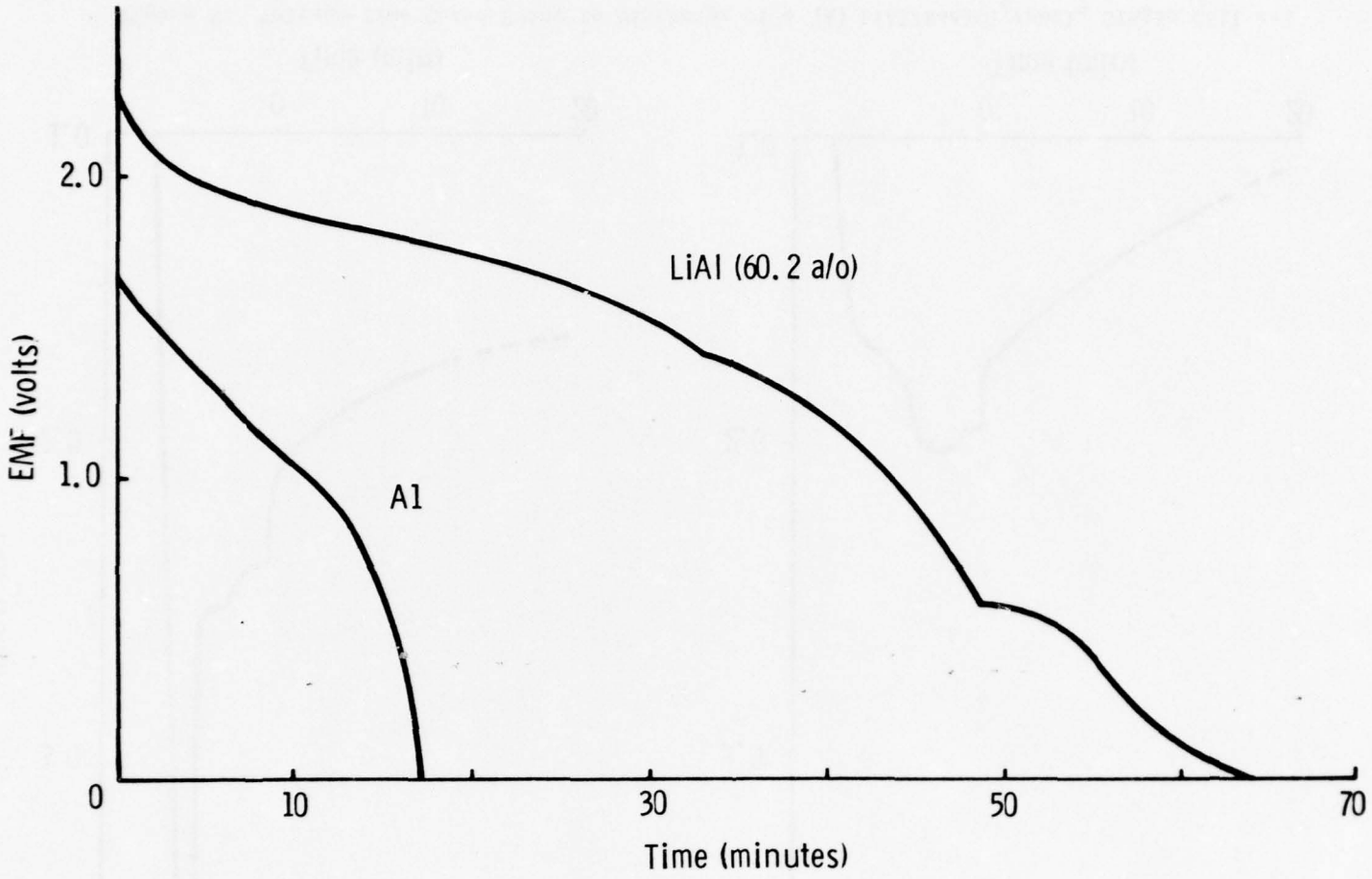

Figure 2. Discharge Curve of a Single Cell Utilizing a LiAl or Al Anode at 25 mA/cm^2 and 175°C

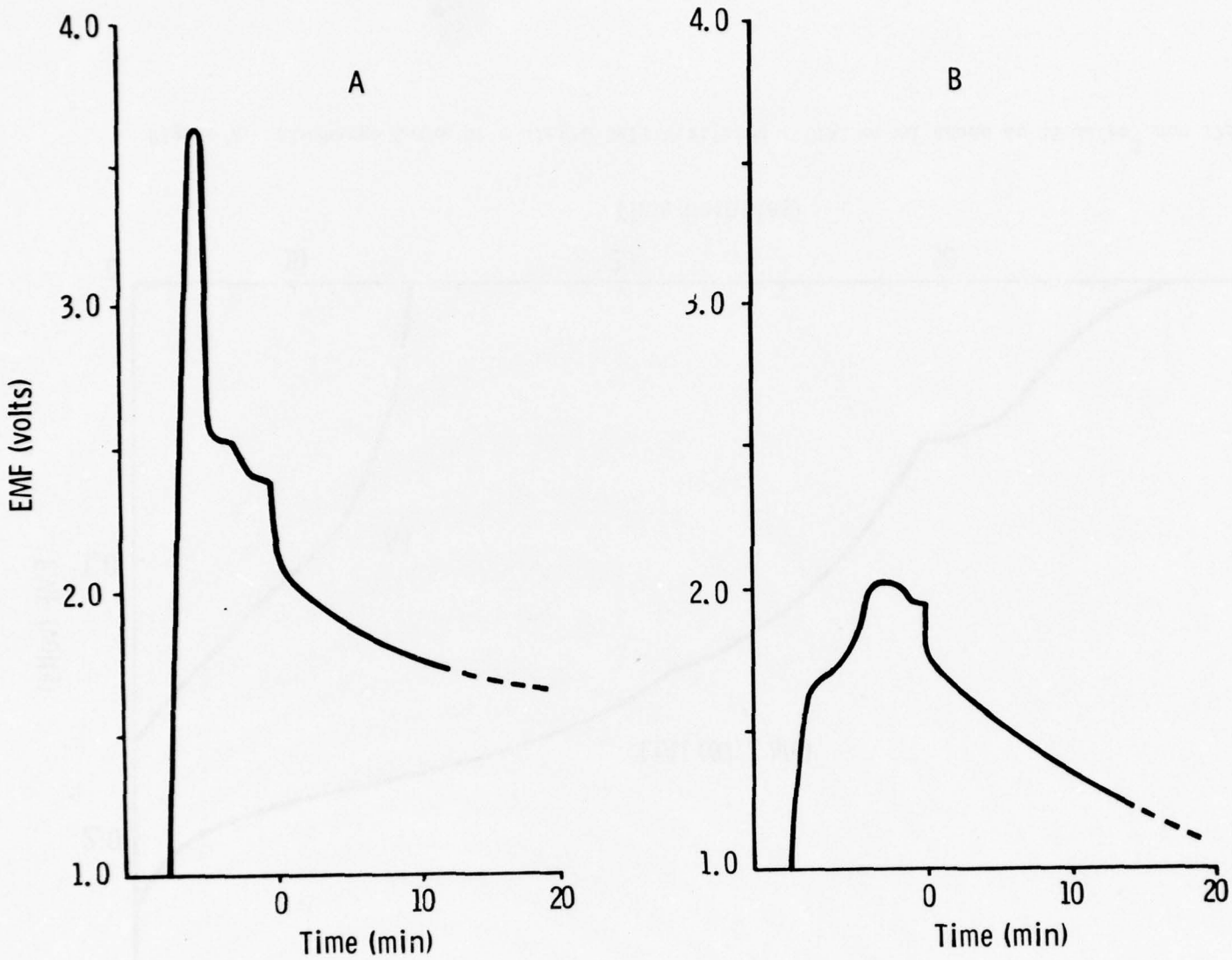

Figure 3. Voltage-Time Curve Prior to Discharge of a (A) LiAl/$NaAlCl_4$/$MoCl_5$ Single Cell and (B) Al/$NaAlCl_4$/$MoCl_5$ Single Cell

both a lithium-boron alloy anode and a pure lithium anode (22). We observed cell behavior during discharge that suggested aluminum is oxidized rather than lithium. This was shown by 1.8V potential established during the self discharge of an optimized single cell (Figure 4). This voltage corresponds to the potential for a pure aluminum anode in this $AlCl_3$-NaCl electrolyte. The use of different atomic percent LiAl alloy anodes (Table III) shows little difference in total energy density output, giving added credence to the suggested functions of lithium in the anode. The performance of the three different LiAl alloys are shown within the limits of Figure 5. Based on total energy density produced during a single cell discharge, the 60.2 a/o LiAl alloy was selected, but the three alloys fell within the 3.25% relative error limits.

The effect of the $MoCl_5$ particle size on overall performance (Figure 6) shows that the highest energy density was obtained with the larger particle size (>30), but using this size resulted in a crumbly catholyte layer with ragged edges. To insure more uniform pellet construction, the 30-50 mesh particle size was selected for the final cell configuration. The improved performance by cells with the larger $MoCl_5$ particle size could be explained assuming that the larger, lower surface area particles dissolve at a slower rate in the electrolyte, and thus diffusional migration to the anode resulting in internal shorting is lessened.

Optimized single cells were subjected to changes in operating temperatures and discharge rates. Constant current discharges of 5, 15, 25, 50, 75, and 100 mA/cm^2, at temperatures of 175, 200, 225, and 250°C, (Figure 7) were used to determine operational parameters. At operating temperatures above the melting point of $MoCl_5$, 194.5°C (25), we observed

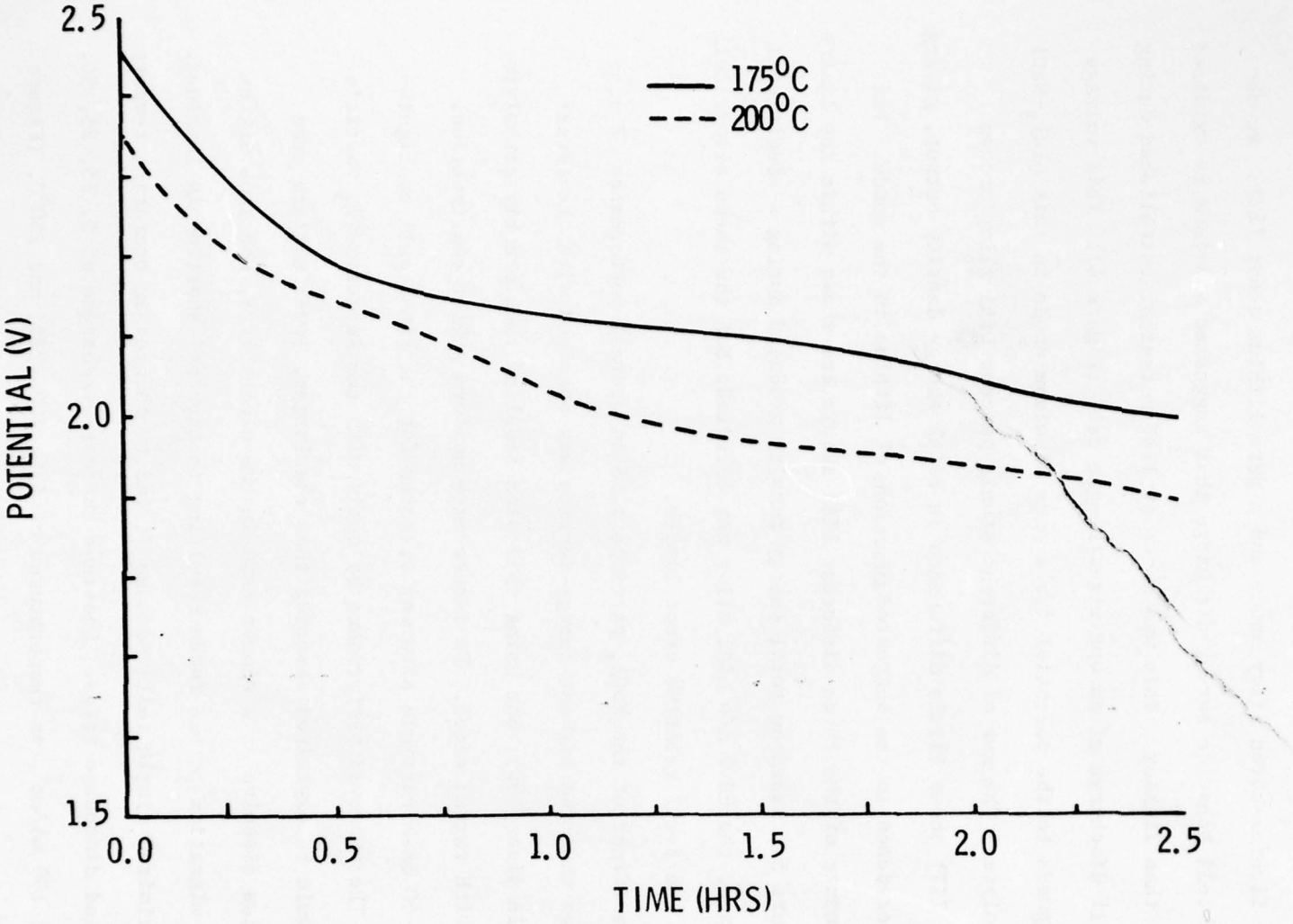

Figure 4. Open-Circuit Discharge of a $LiAl/NaAlCl_4/MoCl_5$ Single Cell at 175°C and 200°C

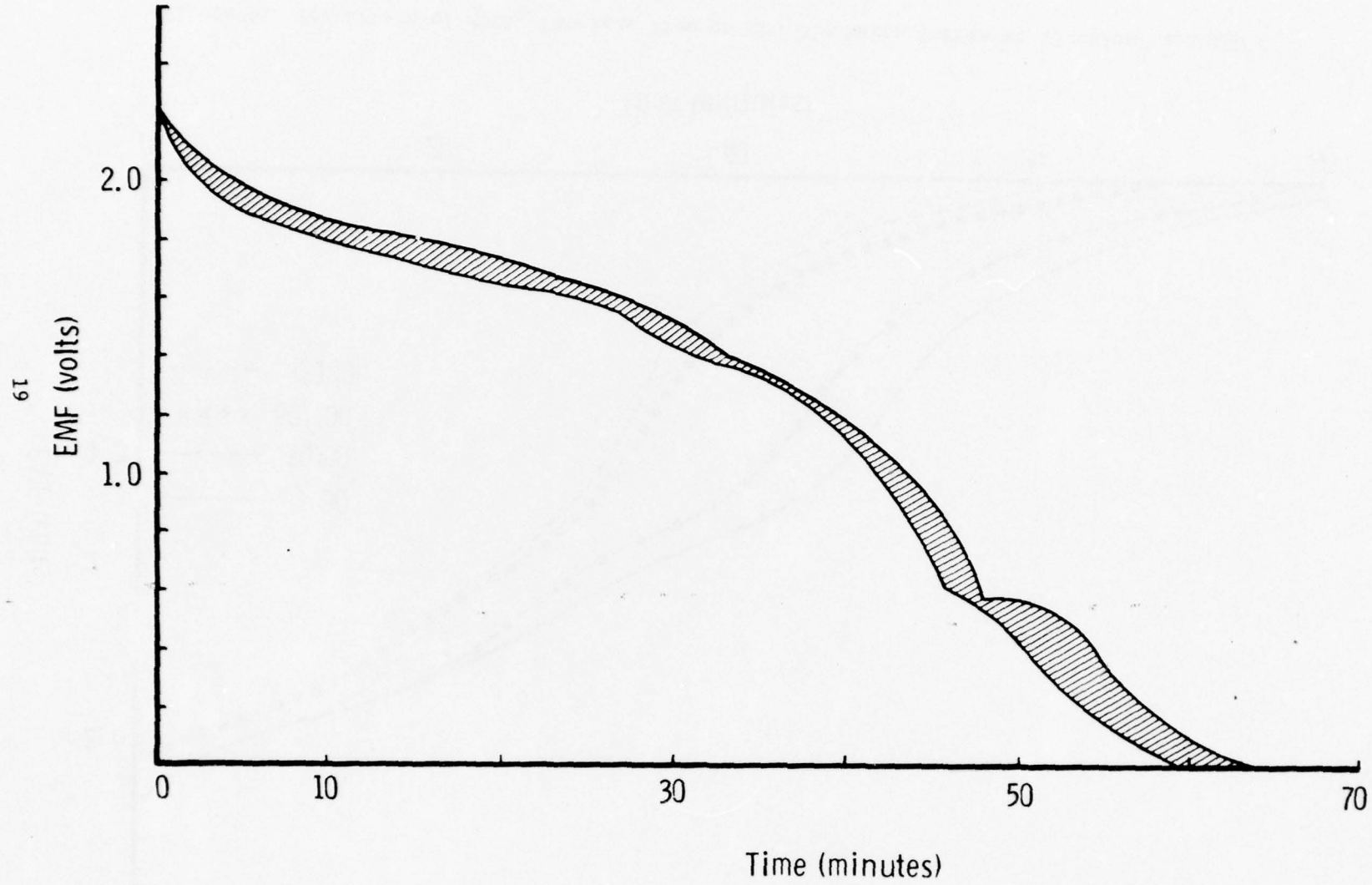

Figure 5. Discharge Performance Envelope for Three Single Cells Utilizing 48.0, 60.2, and 90.9 a/o LiAl Anodes at 25 mA/cm^2 and 200°C

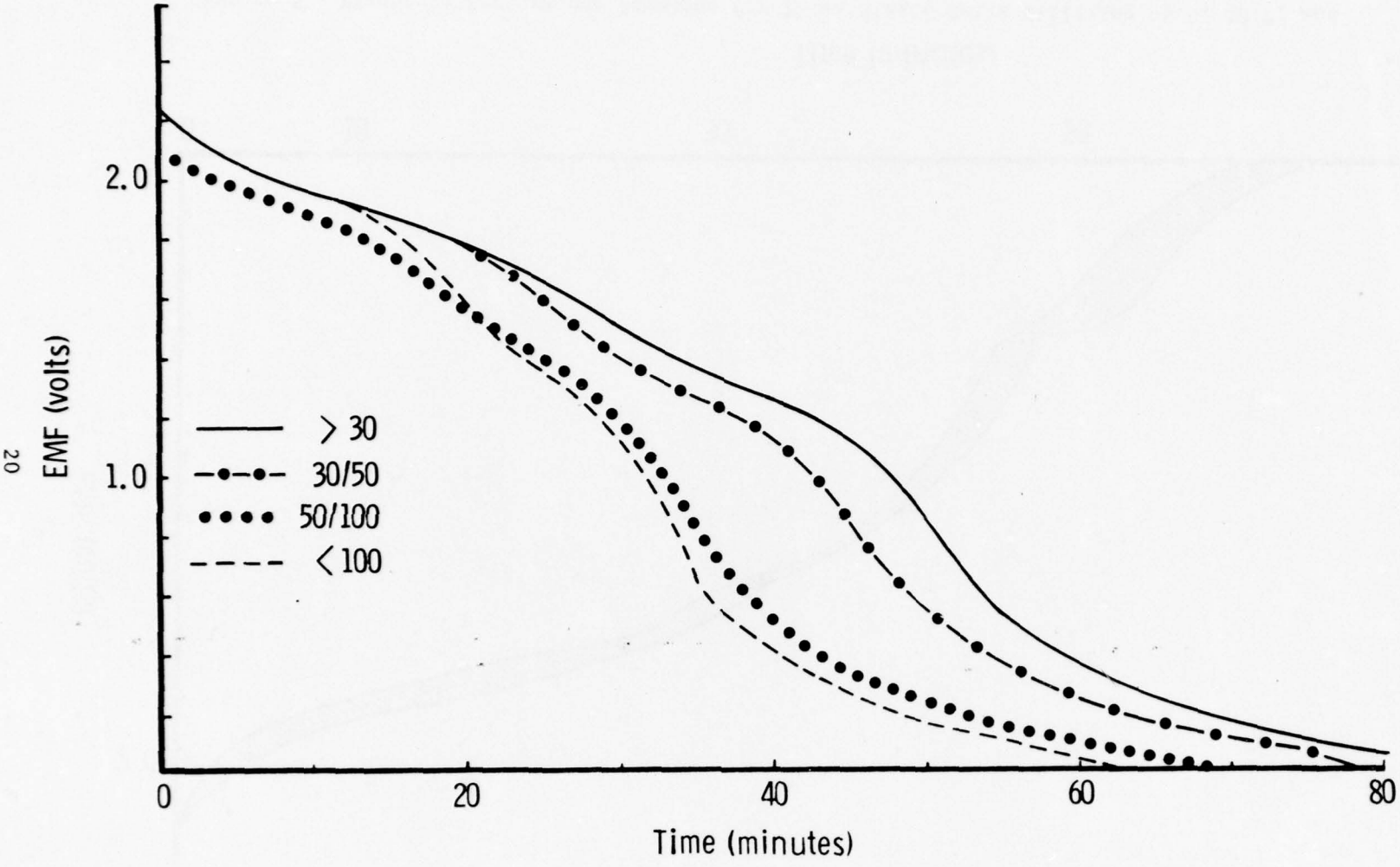

Figure 6. The Effect of $MoCl_5$ Particle Size on the Discharge Curves at 15 mA/cm^2 and 200°C

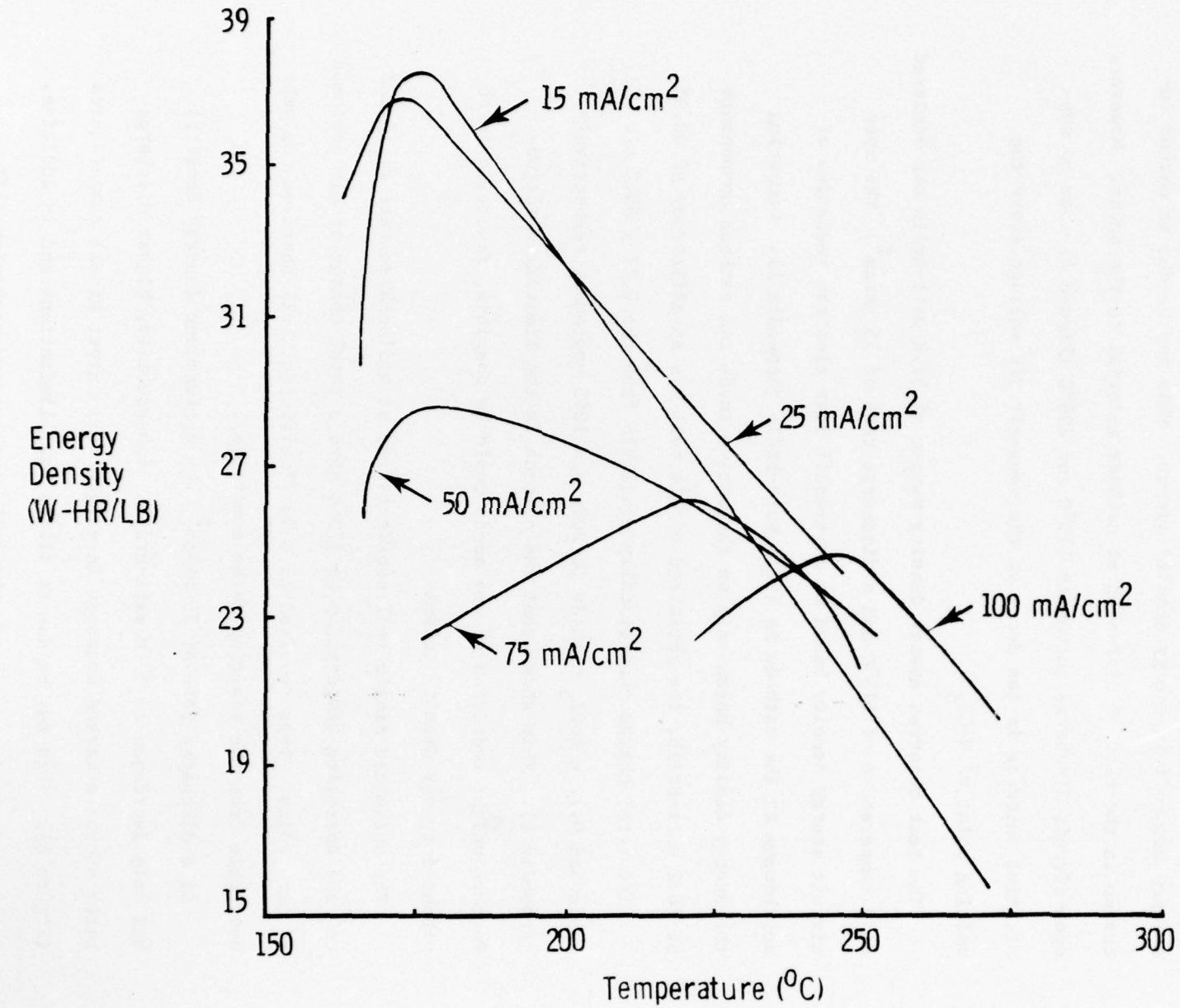

Figure 7. Energy Density as a Function of Temperature at Discharge Rates of 15, 25, 50, 75, and 100 mA/cm^2.

a sharp drop-off in energy density output. This may be due to marked increase in the rate of diffusion of cathode material to the anode. However, open-circuit discharge curves at 175°C and 200°C (Figure 4) show no substantial increase in the decay of the open-circuit voltage above the melting point of $MoCl_5$.

The best observed energy density output of 37.8 watt-hr/lb was achieved at a temperature of 175°C and a discharge rate of 15 mA/cm^2. The open circuit energy density based on an overall five electron reduction of molybdenum at the cathode is 190.4 watt-hr/lb (Appendix A). Comparing the energy density based only on the active anode and cathode components of 76.2 watt-hr/lb, the optimized single cell has an efficiency of 40.0%.

The total charge theoretically available from the 0.27 g 60.2 a/o LiAl anode and 0.72 g $MoCl_5$ cathode is 2086 and 1265 coulombs, respectively (Appendix B). This shows that the cathode is the limiting electrode. Further weight reduction of the anode could be possible, resulting in an enhanced energy density output.

The optimized single cell configuration at a discharge rate of 15 mA/cm^2 and operating temperature of 175°C gave a total charge of 616 coulombs to zero volts. This resulted in a 48.7% efficient cell based on coulombs available from the limiting cathode material.

At a discharge rate of 25 mA/cm^2, the performance (energy density) had only decreased to 37.0 watt-hr/lb. Subsequently, higher discharge rates showed a marked decrease in single cell output at all temperatures (Figure 8). This may be due to diffusional limitations and in addition, interposed chemical steps in the cathode reduction mechanism (15).

Internal resistance is another important factor that must be considered in determining battery performance. It reduces the useful voltage

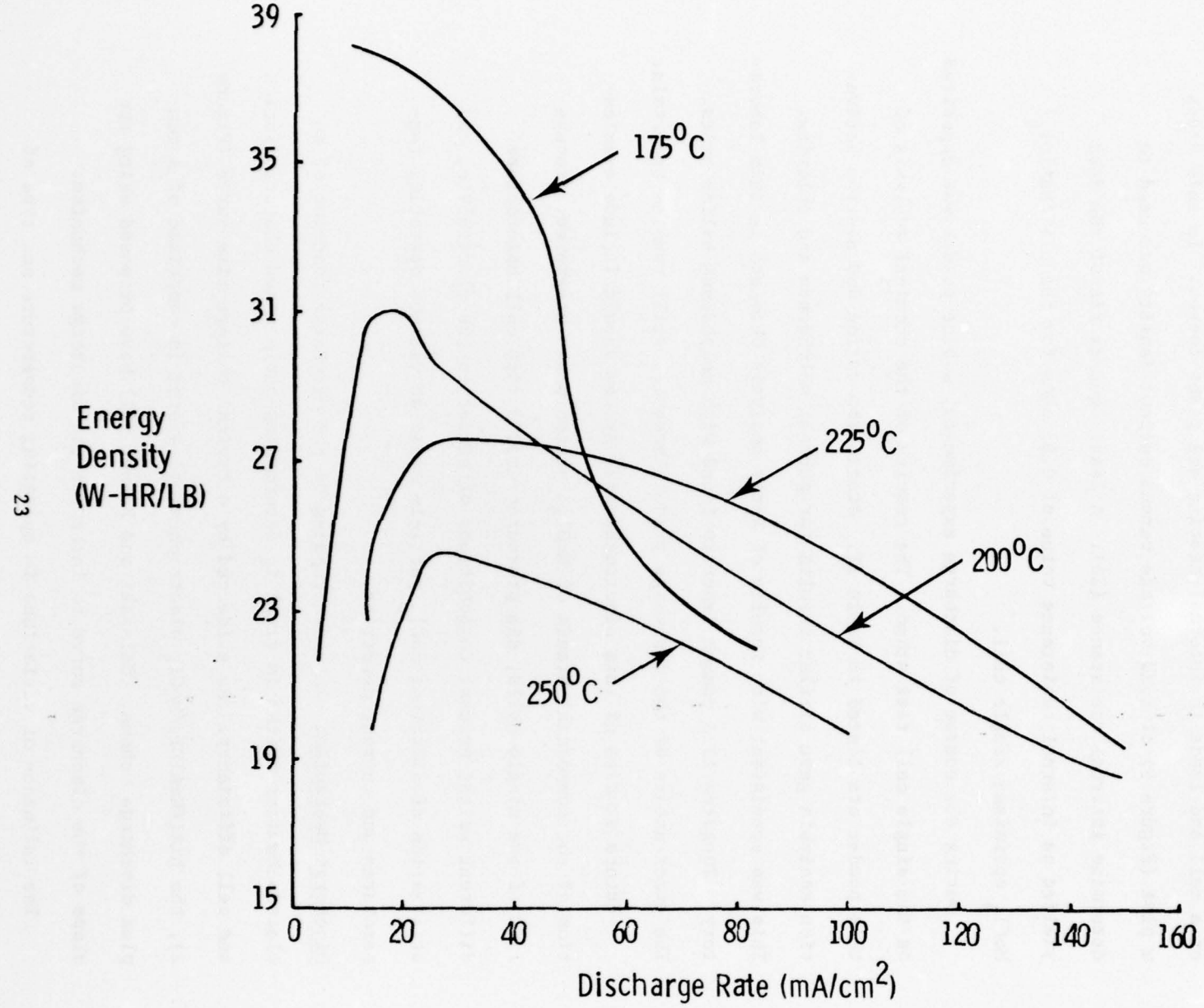

Figure 8. Energy Density as a Function of Discharge Rate at Temperatures of 175, 200, 225, and 250°C

of a cell and leads to internal heating and power losses. In this study a plot (Figure 9) of load voltage versus current density was used to determine internal resistance (26). A least squares fit of the data yielded an internal resistance value of 0.63 ohms for the $LiAl/NaAlCl_4/MoCl_5$ optimized single cell.

During the course of discharge experiments, a blue powder was deposited on the single cell test stand. The results of the chemical analysis of this powder are listed in Table IX. Atomic absorption and neutron activation analysis gave similar results for percent molybdenum and chlorine. This was consistent with results of X-ray analysis obtained in this laboratory. Tungsten is a common impurity found with molybdenum halide salts. The exact nature of the discharge product however, still remains uncertain.

Future studies of this electrochemical system should include examination of the commercial brands of $MoCl_5$, platen press pressures, storage life of the single cells, die pressures used during cell manufacture, different weight percent compositions of binder in the electrolyte, and utilization of different $MoCl_5$ particle sizes at various operating temperatures and current densities.

Discharge Mechanism: An understanding of the discharge reaction of an electrochemical system is vital in determining performance characteristics and cell efficiency. As evidenced by a typical voltage-time curve (Figure 2), the $LiAl/NaAlCl_4/MoCl_5$ electrochemical system is comprised of a complex discharge scheme. Balewski and Brenet (21) have proposed using the slope of the discharge curve to interpret the discharge mechanism.

The influence of variations in operating temperature and type of graphite in the catholyte on the shape of the derivative of the discharge

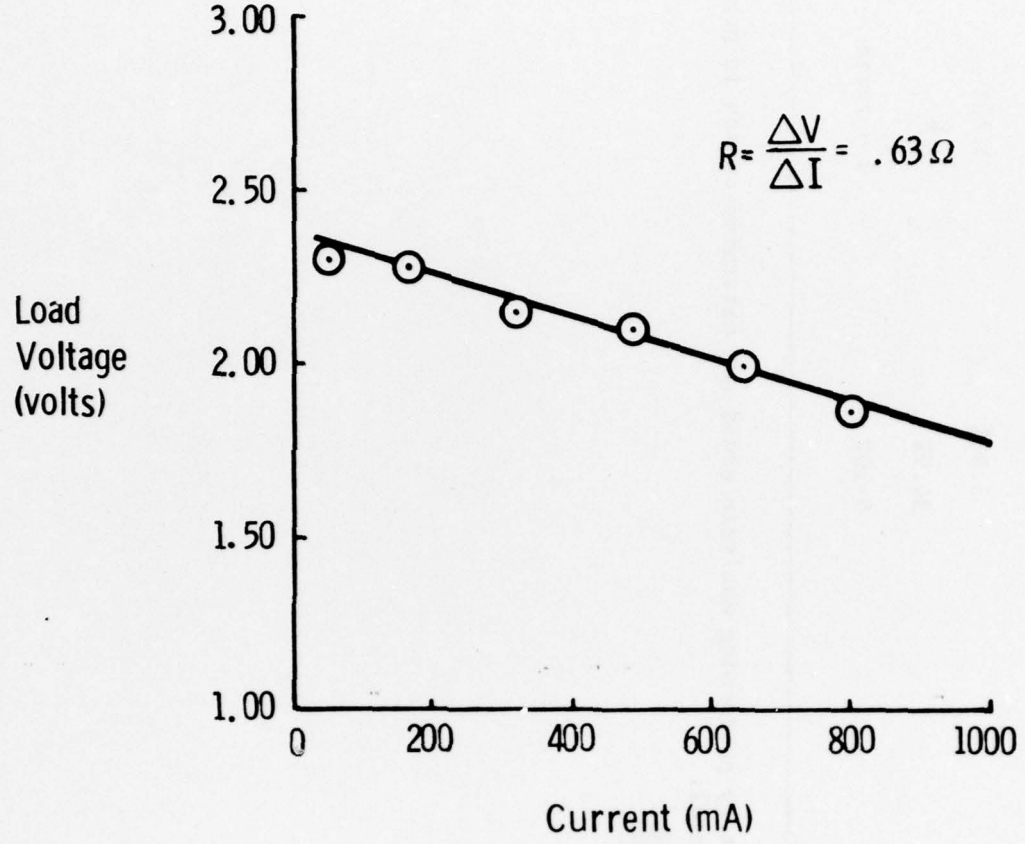

Figure 9. Load Voltage as a Function of Current For a LiAl (60.2 a/o)/$NaAlCl_4$/$MoCl_5$ Single Cell at 25 mA/cm^2 and 200°C

TABLE IX. BLUE POWDER ANALYSIS

	NEUTRON ACTIVATION	ATOMIC ABSORPTION
Mo	54.9%	56.35%
Cl	5.98%	5.70%
O	34.9%	--[a]
W	5-10%	0 - trace

[a]Laboratory performing analysis could not determine oxygen in presence of a metal.

curve was studied using the optimized cell configuration (Figures 10 and 11). The slope was calculated at 100 second intervals, representing a constant increment of 9.6 coulombs.

Figure 10A represents the derivative curve for a single cell discharge at 175°C utilizing Fisher graphite in the catholyte. The curve consists of one major peak (A) centered at 1.91 volts and five smaller peaks (B-F) appearing at different cell voltages and differing in width and total area.

Comparison of the derivative curves at 175°C (Figure 10a) and at 200°C (Figure 10b) shows that the area of peaks A, B, C and E decreased while that of peaks D and F increased with increasing temperature. Furthermore, there is a slight shift in the position of the peaks. At 200°C, the derivative curve is composed of only three major peaks as compared to the six peaks observed at 175°C. At the next higher temperature of 250°C, peak G decreased while peaks H and J appear to have combined into the more distinguishable peaks L-P. A comparison of the areas under the individual peaks shows that as the operating temperature is increased the major supporting reactions occur at lower potentials. For example, the discharge step represented by peak A contributed approximately 38% of the total charge delivered at 175°C. This percentage decreased to 29% at 200°C (peak G) and finally to 22% at 250°C (peak K). Only 27% of the total coulombs were supplied below 0.8V by the single cell discharged at 175°C. This value successively increased to 40% and 54% at temperatures of 200°C and 250°C respectively. In an operational battery configuration, voltage constraints often require voltage cutoffs be 80% peak voltage. If one were to apply this criteria to single cell experiments, this would indicate an optimized single cell operating temperature of 175°C.

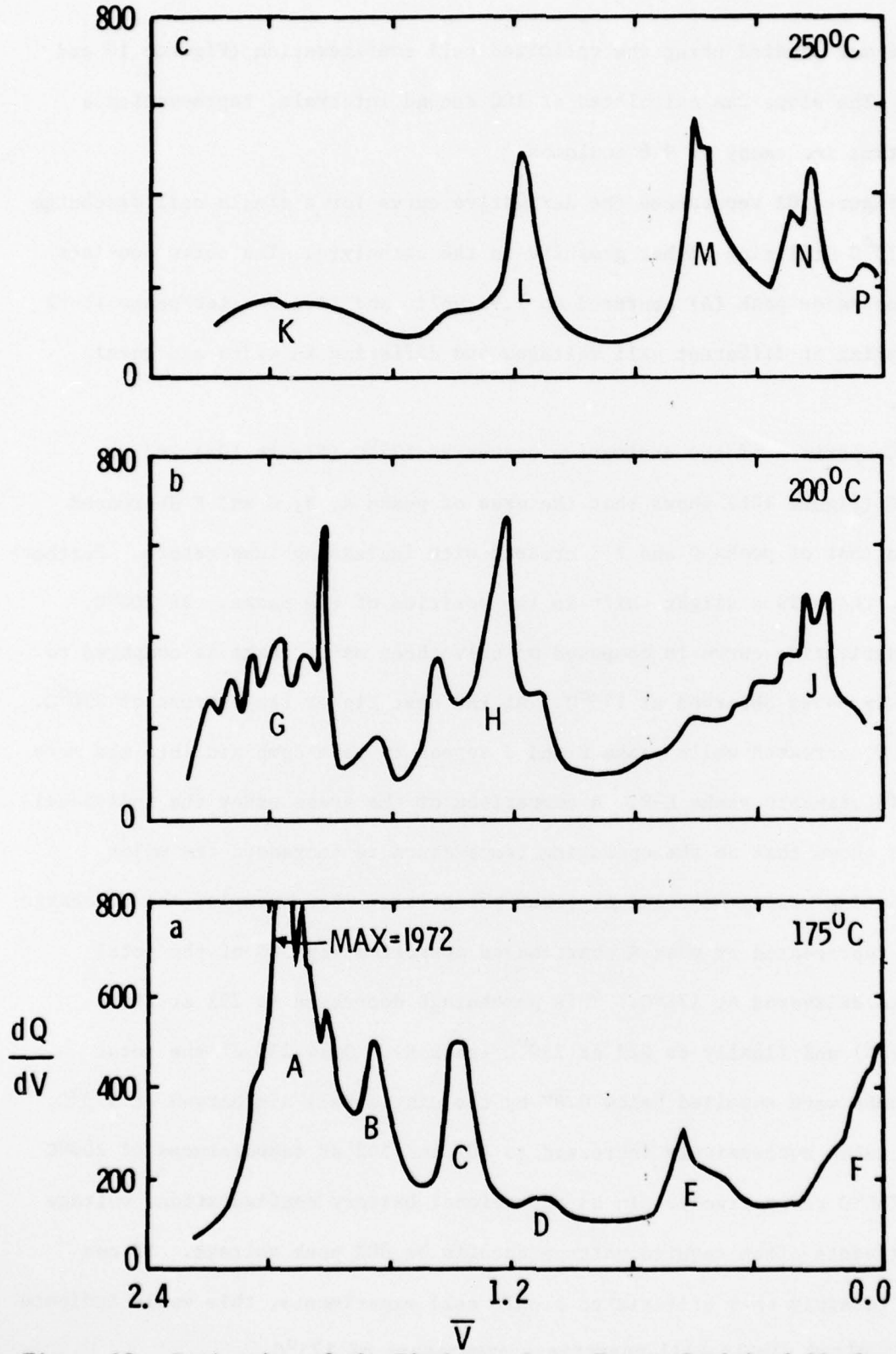

Figure 10. Derivative of the Discharge Curve For an Optimized Single Cell Utilizing Fisher Graphite in the Catholyte

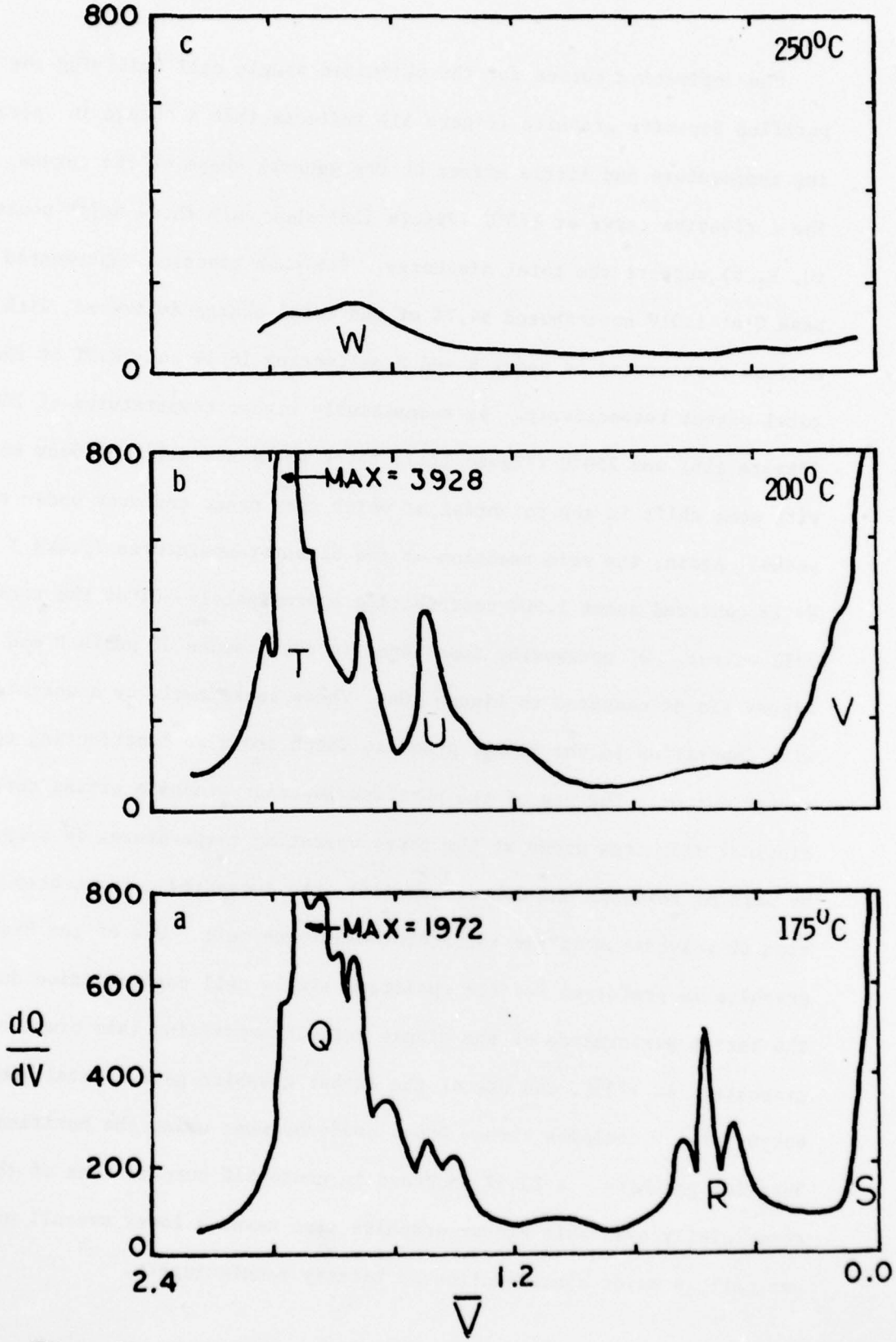

Figure 11. Derivative of the Discharge Curve For an Optimized Single Cell Utilizing Purified Superior Graphite in The Catholyte

The derivative curves for the optimized single cell utilizing the purified Superior graphite (Figure 11) indicate that a change in operating temperature had little effect on the general shape of the curves. The derivative curve at 175°C (Figure 11a) show only three major peaks (Q, R, S) support the total discharge. The main reaction represented by peak Q at 1.91V contributed 54.7% of the total charge delivered, with reactions represented by peaks R and S delivering 16.4% and 28.9% of the total output respectively. At successively higher temperatures of 200°C (Figure 11b) and 250°C (Figure 11c), three peaks are still evident but with some shift in the potential at which they occur and area under the peaks. Again, the main reaction at the higher temperatures (peaks T and W) is centered about 1.90V contributing approximately 50% of the total cell output. Of noteworthy importance is the absence of peaks B and C in Figure 11a as compared to Figure 10a. These peaks could be associated with impurities in the Fisher graphite which are also contributing to total charge output. The use of the purified Superior graphite giving three distinct discharge steps at the three operating temperatures is supported by work of Phillips and Osteryoung (15), who suggested a three-step reduction of molybdenum in the tetrachloroaluminate melt. Use of the Fisher graphite is preferred for the optimized single cell configuration due to the better performance of the single cell incorporating this brand of graphite. At 175°C, the use of the Fisher graphite gave a total charge output of 616 coulombs versus 498.5 coulombs when using the purified Superior graphite - a 23.5% increase in coulombic output. Use of the commercially available Fisher graphite also means a lower overall price per cell, a major consideration by battery manufacturers.

CONCLUSION

This work demonstrates a practical improvement in thermal batteries. Low temperature thermal battery single cells are described which employ lithium-aluminum anodes, molybdenum pentachloride cathodes, and a NaCl-saturated $AlCl_3$-NaCl electrolyte.

Experimental results suggest a cell optimized for maximum energy density output consists of a 60.2 a/o liAl anode, and a cathode of 30-50 ASTM mesh particle size $MoCl_5$, and Fisher graphite separated by a NaCl-saturated $AlCl_3$-NaCl electrolyte.

The operating conditions for maximum output exist at current densities of 15-25 mA/cm^2 at temperatures of 175-200°C, with a calculated internal resistance of 0.63 ohms. Preliminary cost estimates (27) in a multicell cell battery indicate this system to be a viable competitor for current state of the art thermal batteries with the added advantage of lower operating temperatures.

The first use of the derivative of the discharge curve in thermal battery analysis substantiates the complexity of the discharge. Use of this function gives an insight into the temperature dependence of the $LiAl/MoCl_5$ couple in the supporting electrolyte and utilization of various commercial brands of graphite in the catholyte.

REFERENCES

1. S.M. Seilis, L.P. McGinnis, E.S. McKee, and J.T. Smith, J. Electrochem. Soc., 110, 469 (1963).

2. S.M. Seilis, J.F. Wondowski, and R.F. Justus, ibid, 111, 6 (1964).

3. H. Goldsmith and J.T. Smith, Electrochem. Technol., 6, 16 (1968).

4. L.H. Thaller, J. Electrochem. Soc., 115, 116 (1968).

5. B.H. Van Domelen and R.D. White, "A Review of Thermal Battery Technology," Proc. Ninth Intersociety Energy Conversion Engineering Conference, 1974.

6. C.W. Jennings, "Thermal Batteries," The Primary Battery, Vol. Two, N.C. Cahoon and C.W. Heise, Ed., John Wiley and Sons, Inc., New York, NY, 1976, pp 263-293.

7. B.W. Mulligan, "Low Temperature Thermal Batteries," Proc. Twenty-seventh Power Sources Symposium, PSC Publication Committee, Red Bank, NJ, 1976, pp 147-151.

8. G.D. Brabson, J.K. Erbacher, L.A. King, and D.W. Seegmiller, FJSRL Technical Report 76-0002, F.J.Seiler Research Laboratory (AFSC) USAF Academy, CO, 1976.

9. R.H. Moss, PhD Thesis, University of Connecticut, 1955.

10. R.C. Howie and D. W. Macmillan, J. Inorg. Nucl. Chem., 33, 3681 (1971).

11. C.L. Hussey, J.K. Erbacher, and L.A. King, FJSRL Technical Report 76-0003, F.J. Seiler Research Laboratory (AFSC), USAF Academy, CO, 1976.

12. S. Senderoff and A. Brenner, J. Electrochem. Soc., 101, 16 (1954).

13. E.E. Marshall and L.F. Yntema, J. Phys. Chem., 46, 353 (1952).

14. T. Suzuki, Electrochim Acta, 15, 127 (1970).

15. J. Phillips and R.A. Osteryoung, Colorado State University, unpublished manuscript, 1976.

16. L. Campanella and G. Pistonia, J. Electrochem. Soc., 118, 1905 (1971).

17. L. Campanella and G. Pistonia, ibid, 120, 383 (1973).

18. F.W. Dampier, ibid, 121, 656 (1974).

19. B. DiPietro, V. Filippeschi, M. Lazzari, G. Pistonia, and B. Scrosati, Paper No. 34; presented at the Tenth International Power Sources Symposium, Brighton, England, September 1976.

20. T. Valand, J. Power Sources, 1, 65 (1976).

21. L. Balewski and J.P. Brenet, Electrochem. Technol., 5, 527 (1967).

22. J.K. Erbacher, C.L. Hussey, and L.A. King, FJSRL Technical Report 77-0001, F.J. Seiler Research Laboratory (AFSC), USAF Academy, CO, 1977.

23. H.C. Strobel, "Chemical Instrumentation: A Systemic Approach," Addison-Wesley Publishing Company, Reading, MA, 1973, pp 11-13.

24. D.M. Bush, "Results of Thermal Battery Testing," Proc. Twenty-Sixth Power Sources Symposium, PSC Publication Committee, Red Bank, NJ, 1974, pp 144-147.

25. W.J. Hamer, "Internal Resistance of Primary Batteries," The Primary Battery, Vol. Two, N.C. Cahoon and G.W. Heise, Ed., John Wiley and Sons, Inc., New York, NY, 1976, pp 429-460.

26. J.A. Dean, Ed., Lange's Handbook of Chemistry, 11th Edition, McGraw-Hill, Inc., New York, NY, 1973, p 4-81.

27. R.A. Marsh, Air Force Aero Propulsion Laboratory, Wright-Patterson AFB, OH, private communication, 1977.

APPENDIX A

Based on the following assumed reaction with an open-circuit voltage of 2.39 volts:[a]

$$5[Al + 4NaCl \rightarrow NaAlCl_4 + 3e^-]$$

$$3[5e^- + MoCl_5 \rightarrow Mo + 5Cl^-]$$

$$5Al + 5NaCl + 3MoCl_5 \rightarrow 5NaAlCl_4 + 3Mo$$

Energy Density = 190.4 watt-hr/lb

The optimized single cell configuration (Table I) has a total weight of 2.64 g. The calculated energy density, based on a consumed anode weight of 0.17 g, a consumed cathode weight of 0.72 g $MoCl_5$, and a required 0.42 g NaCl, is 76.2 W-Hr/lb.

$$\text{Energy Density} = (37.8 \text{ W-Hr/lb}) \frac{2.64 \text{ g}}{1.31 \text{ g}} = 76.2 \text{ W-Hr/lb}$$

$$\text{Efficiency} = \frac{76.2 \text{ W-Hr/lb.}}{190.4 \text{ W-Hr/lb}} (100) = 40.0\%$$

[a]Examples of such calculations are given in the Appendix of Reference 11.

APPENDIX B

Assuming an aluminum anode, the theoretical coulombs available using the optimized 0.27 g 60.2 a/o LiAl alloy is:

$$(0.27 \text{ g LiAl})\left(\frac{.72 \text{ g Al}}{1.00 \text{ g LiAl}}\right)\left(\frac{3e^-}{\text{mole}}\right)\left(\frac{1 \text{ mole}}{26.98 \text{ g Al}}\right)\left(\frac{96{,}487 \text{ coul}}{e^-}\right) =$$

2086. coulombs

Theoretical coulombs based on the optimized 0.72 g $MoCl_5$ cathode assuming an overall 5 electron reduction is:

$$(0.72 \text{ g } MoCl_5)\left(\frac{1 \text{ mole}}{273.12 \text{ g } MoCl_5}\right)\left(\frac{5e^-}{\text{mole}}\right)\left(\frac{96{,}487 \text{ coul}}{e^-}\right)(.955 \text{ purity}) =$$

1272. coulombs

With an experimentally observed value of 616 coulombs for the optimized single cell at 15 mA/cm^2 discharge rate and 175°C, the coulombic efficiency based on the limiting electrode is:

$$\frac{616 \text{ coulombs}}{1272 \text{ coulombs}}\ (100) = 48.4\%$$